Molecular Pharmacology Fast Forward. Published on October 21, 2015 as DOI: 10.1124/mol.115.100891
This article has not been copyedited and formatted. The final version may differ from this version.

Inactivation of Human Cytochrome P450 3A4 and 3A5 by Dronedarone and N-Desbutyl Dronedarone

Yanjun Hong, Yvonne Mei Fen Chia, Ray Hng Yeo, Gopalakrishnan Venkatesan, Siew Kwan Koh, Christina Li Lin Chai, Lei Zhou, Pipin Kojodjojo and Eric Chun Yong Chan

Department of Pharmacy, Faculty of Science, National University of Singapore, 18 Science Drive 4, Singapore 117543 (Y.H., Y.M.F.C., R.H.Y., G.V., C.L.L.C., E.C.Y.C.); Singapore Eye Research Institute, The Academia, 20 College Road Discovery Tower Level 6, Singapore 169856 (S.K.K., L.Z.) and Department of Cardiology and Cardiac Electrophysiology, National University Heart Centre, 5 Lower Kent Ridge Road, Singapore 119074 (P.K.)

Molecular Pharmacology Fast Forward. Published on October 21, 2015 as DOI: 10.1124/mol.115.100891
This article has not been copyedited and formatted. The final version may differ from this version.

Running Title:

Inactivation of CYP3A4 and CYP3A5 by Dronedarone and N-Desbutyl Dronedarone

Address correspondence to:

Associate Professor Eric Chun Yong Chan, Department of Pharmacy, Faculty of Science, National University of Singapore, 18 Science Drive 4, Singapore 117543, Singapore. Email: phaccye@nus.edu.sg

Number of Text Pages	33
Number of Tables	5
Number of Figures	8
Number of References	26
Number of Words in Abstract	246
Number of Words in the Introduction	626
Number of Words in the Discussion	1490

ABBREVIATIONS

AF: Atrial fibrillation

CYP3A4: Cytochrome P450 3A4 enzyme

CYP3A5: Cytochrome P450 3A5 enzyme

CYP450: Cytochrome P450 enzymes

DDIs: Drug-drug interactions

HLM: Human liver microsomes

K_I: Inactivator concentration at half maximum rate of inactivation

Molecular Pharmacology Fast Forward. Published on October 21, 2015 as DOI: 10.1124/mol.115.100891
This article has not been copyedited and formatted. The final version may differ from this version.

k_{Inact}: Inactivation rate constant at infinite inactivator concentration

k_{obs}: Observed inactivation rate constant

LC/MS/MS: Liquid chromatography tandem mass spectrometry

UPLC: Ultra Performance Liquid Chromatography

QTOF/MS: Quadrupole time-of-flight mass spectrometer

MBI: Mechanism-based inactivation

MI Complex: Metabolite-intermediate complex

NDBD: *N*-desbutyl dronedarone

Molecular Pharmacology Fast Forward. Published on October 21, 2015 as DOI: 10.1124/mol.115.100891
This article has not been copyedited and formatted. The final version may differ from this version.

ABSTRACT

Dronedarone is an antiarrhythmic agent approved in 2009 for the treatment of atrial fibrillation. In-house preliminary study demonstrated that dronedarone inhibits CYP3A4 and CYP3A5 in a time-dependent manner. This study aimed to investigate the inactivation of CYP450 by dronedarone. We demonstrated for the first time that both dronedarone and its main metabolite, *N*-desbutyl dronedarone (NDBD), inactivate CYP3A4 and CYP3A5 in a time-, concentration-, and NADPH-dependence manner. For inactivation of CYP3A4, K_I and k_{Inact} are 0.87 μM and 0.039 min^{-1} respectively for dronedarone, and 6.24 μM and 0.099 min^{-1} respectively for NDBD. For CYP3A5 inactivation, K_I and k_{Inact} are 2.19 μM and 0.0056 min^{-1} for dronedarone, and 5.45 μM and 0.056 min^{-1} for NDBD. The partition ratios for the inactivation of CYP3A4 and CYP3A5 by dronedarone are 51.1 and 32.2, and by NDBD are 35.3 and 36.6. Testosterone protected both CYP3A4 and CYP3A5 from inactivation by dronedarone and NDBD. While the presence of Soret peak confirmed the formation of quasi-irreversible metabolite-intermediate (MI) complex between dronedarone/NDBD and CYP3A4/5, partial recovery of enzyme activity by potassium ferricyanide illuminated an alternative irreversible mechanism-based inactivation (MBI). MBI of CYP3A4 and CYP3A5 was further supported by the discovery of GSH adducts derived from the quinone oxime intermediates of dronedarone and NDBD. In conclusion, dronedarone and NDBD inactivate CYP3A4 and CYP3A5 via unique dual mechanisms of MBI and formation of MI complex. Our novel findings contribute new knowledge for future investigation of the underlying mechanisms associated with dronedarone-induced hepatotoxicity and clinical drug-drug interactions (DDIs).

Molecular Pharmacology Fast Forward. Published on October 21, 2015 as DOI: 10.1124/mol.115.100891
This article has not been copyedited and formatted. The final version may differ from this version.

INTRODUCTION

Atrial fibrillation (AF) is the most common sustained arrhythmia in aging population and is associated with increased cardiovascular morbidity and mortality (Trigo and Fischer, 2012). With the rapid growth of elderly population, the prevalence of AF is substantially increasing, resulting in a major public-health problem. Despite several developments in antithrombotic, antiatherosclerotic and device-based cardiac therapies, few noteworthy antiarrhythmic drugs have been developed (Pamukcu and Lip, 2011). Dronedarone (Fig. 1A) is the only antiarrhythmic drug approved in 2009 by the US Food and Drug Administration (FDA) since 1999 (De Ferrari and Dusi, 2012). The pharmacological effects of dronedarone are derived from its electrophysiological properties belonging to all four Vaughan-Williams classes (Oyetayo et al., 2010). It is a non-iodinated benzofuran derivative of amiodarone (Fig. 1B) and was developed with the intention of improving the safety profile of rhythm-controlling drugs (De Ferrari and Dusi, 2012).

Despite the promises of dronedarone as a safer alternative to amiodarone, post-marketing surveillance revealed that it is not entirely without adverse effects. In January 2011, FDA released a drug safety alert for dronedarone due to reported cases of severe liver injury, including two cases of acute liver failure leading to liver transplant (USFDA, 2011). Most recently, there have been a number of reports on significant drug-drug interactions (DDIs) involving dronedarone. The coadministration of dronedarone and simvastatin increased simvastatin levels by 4-fold (Patel et al., 2009). The docetaxel-dronedarone interaction led to grade 4 neutropenia and mucositis which was probably related to increased systemic exposure of docetaxel (Vodovar et al., 2011). In addition, there were cases of arrhythmic death among patients treated with dronedarone, which might be related to the pharmacokinetic interaction between dronedarone and digoxin (De Ferrari and Dusi, 2012).

Dronedarone undergoes extensive hepatic metabolism by cytochrome P450 enzymes (CYP450) (Ferrari and Dusi, 2012). *N*-desbutyl dronedarone (NDBD, Fig. 1C), the main metabolite formed primarily by CYP3A, is pharmacologically active and has similar plasma exposure to its parent drug

Molecular Pharmacology Fast Forward. Published on October 21, 2015 as DOI: 10.1124/mol.115.100891
This article has not been copyedited and formatted. The final version may differ from this version.

(Klieber et al., 2014). While the overall metabolic pathway of dronedarone has been reported recently (Klieber et al., 2014), no study investigates the mechanism of inhibition of CYP450 by dronedarone thus far.

As a structural analog of amiodarone, dronedarone retains the tertiary amine group and its associated potential to be oxidized to a nitroso intermediate that may in turn form a metabolite-intermediate (MI) complex with the heme iron of CYP450 (Delaforge et al., 1983; Mansuy et al., 1976). Such quasi-irreversible inactivation of CYP450 could lead to the accumulation of co-administered drug that is a substrate of the same CYP450, and subsequently result in adverse effects arising from DDIs (Grimm et al., 2009). In fact, amiodarone has been shown to cause time-dependent inhibition of CYP3A4 (Ohyama et al., 2000) and CYP2C8 (Polasek et al., 2004), a key feature of irreversible or quasi-irreversible inactivation of CYP450. Although dronedarone has been reported to be a moderate inhibitor of CYP3A4 and a weak inhibitor of CYP2D6 (Naccarelli et al., 2011), the potential inactivation of CYP450 by dronedarone and NDBD has not been investigated. In-house preliminary findings demonstrated that dronedarone inhibits CYP3A4 and CYP3A5 in a time-dependent manner (data not shown). Based on these collective evidences, we hypothesize that dronedarone and its main metabolite, NDBD, have the propensity to inactivate CYP450.

In the present study, the mechanism of inactivation of CYP3A4 and CYP3A5 by dronedarone and NDBD was investigated. Metabolic stability, enzyme kinetics and CYP450 reaction phenotyping experiments were performed to identify the major CYP450 responsible for dronedarone metabolism. Metabolite identification was further performed to establish the key metabolites of dronedarone when metabolized by CYP3A4 and CYP3A5. The nature of enzyme inactivation was subsequently characterized based on time-, concentration-, NADPH-dependent inhibition, substrate protection and spectral difference scanning experiments. GSH-trapping experiments were further conducted to trace the potential reactive metabolites associated with dronedarone and NDBD.

Molecular Pharmacology Fast Forward. Published on October 21, 2015 as DOI: 10.1124/mol.115.100891
This article has not been copyedited and formatted. The final version may differ from this version.

MATERIALS AND METHODS

Chemicals. High-performance liquid chromatography-grade acetonitrile (ACN) was purchased from Tedia Company Inc. (Fairfield, OH). Dronedarone hydrochloride, NDBD, verapamil hydrochloride, erythromycin, carbamazepine, ketoconazole, prednisolone, testosterone and amodiaquin dihydrochloride dihydrate were purchased from Sigma-Aldrich (St. Louis, MO); diclofenac potassium, debrisoquine sulfate, mephenytoin and phenacetin were obtained from MP Biomedicals (Santa Ana, CA); chlorzoxazone was purchased from Alfa Aesar (Ward Hill, MA); midazolam was purchased from Tocris Bioscience (Bristol, UK); 6β-hydroxytestosterone and 1'-hydroxymidazolam were obtained from Cerilliant Corporation (Round Rock, TX); potassium ferricyanide was purchased from VWR International (Leuven, Belgium). Pooled human liver microsomes (HLM), human recombinant CYP supersomes (rCYP enzymes; with the exception of rCYP2C9) and NADPH regenerating system consisting of NADPH A ($NADP^+$ and glucose 6-phosphate) and B (glucose-6-phosphate dehydrogenase) were purchased from BD Gentest (Woburn, MA). rCYP2C9 was obtained from Cypex (Dundee, UK). Water was obtained using a Milli-Q water purification system (Millipore, Billerica, MA). All other reagents were of analytical grade.

Metabolic Stability Study. HLM (0.5 mg/mL) were pre-incubated with potassium phosphate buffer (100 mM, pH 7.4), NADPH B and dronedarone (1 μM) at 37°C for 5 min. NADPH A was subsequently added to initiate the reaction (i.e. 0 min). The final incubation mixture had a total volume of 400 μL and contained < 1% v/v organic solvent. The reaction mixtures were incubated at 37°C with gentle agitation. At the respective time points (0, 5, 15, 30, 45 and 60 min), 55 μL of the reaction mixture was quenched using ice-cold ACN with verapamil as the internal standard (IS). The samples were then centrifuged at 15 000 *g* and 4°C for 10 min and 80 μL of each supernatant was transferred to a LC/MS vial. Incubation experiments with verapamil (and dronedarone as the IS) were carried out as the positive control. A third set of incubation mixtures containing Milli-Q water in place of NADPH served as the negative control. The loss of parent compound (i.e. dronedarone as the test

Molecular Pharmacology Fast Forward. Published on October 21, 2015 as DOI: 10.1124/mol.115.100891
This article has not been copyedited and formatted. The final version may differ from this version.

compound or verapamil as the positive control) was determined over time using LC/MS/MS analysis. All samples were analyzed in triplicates.

Enzyme Kinetics Study. For the enzyme kinetics study, incubation experiments were carried out using 96-well plates. Incubation mixtures consisting of 0.5 mg/mL HLM, 100 mM potassium phosphate buffer (pH 7.4), NADPH B and dronedarone (0, 1, 5, 10, 20, 50, 75 and 100 μM) were pre-warmed at 37°C for 5 min. Subsequently, the reaction was initiated with the addition of NADPH A. The final volume in each well was 100 μL and the total organic concentration of each incubation mixture was < 1% v/v acetonitrile. At 15 min after the addition of NADPH A, the reaction was quenched using 0.1 μM verapamil in ice-cold ACN before centrifugation at 15 000 *g* and 4°C for 10 min. The peak area ratio of NDBD (with verapamil as the IS) formed with different concentration levels of dronedarone was determined using LC/MS/MS analysis. The corresponding concentration levels of NDBD formed were determined by correlating the peak area ratio obtained to the standard curve obtained with NDBD (0.1, 1, 10, 100 and 1000 nM) subjected to the same conditions as the incubation mixtures. All experiments were performed in triplicates.

Cytochrome P450 Reaction Phenotyping Assay. Dronedarone was incubated with rCYP450 to determine the *in vitro* biotransformation of dronedarone and to elucidate the proportion of hepatic metabolism that is accounted for by the various CYP450 enzymes. Each incubation mixture consisted of dronedarone (3 μM) and NADPH B in 100 mM potassium phosphate buffer (pH 7.4). Each of these rCYP450 (rCYP3A4, rCYP3A5, rCYP2C8, rCYP2C9, rCYP2C19, rCYP2E1, rCYP1A2 or rCYP2D6) was added to obtain a final enzyme concentration of 20 pmol/mL. After pre-warming the incubation mixture at 37°C for 5 min, NADPH A was added to initiate the metabolic reaction. The final incubation mixture volume was 400 μL with < 1% v/v organic phase. At fixed incubation time points (0, 5, 15, 30, 45 and 60 min), 55 μL of the reaction mixture was quenched with 0.1 μM verapamil in ice-cold ACN. All quenched samples were centrifuged at 15 000 *g* and 4°C for 10 min. Positive and negative controls were tested for each experiment. For the positive control, FDA-recommended CYP substrates were used in place of dronedarone. The specific substrates are testosterone (CYP3A4 &

Molecular Pharmacology Fast Forward. Published on October 21, 2015 as DOI: 10.1124/mol.115.100891
This article has not been copyedited and formatted. The final version may differ from this version.

CYP3A5), amodiaquine (CYP2C8), diclofenac (CYP2C9), S-mephenytoin (CYP2C19), chlorzoxazone (CYP2E1), phenacetin (CYP1A2) and debrisoquine (CYP2D6). The final substrate concentration in the incubation mixture was 1 μM. For the negative control, NADPH was replaced with an equal volume of Milli-Q water. The percentage of substrate remaining at each time point was measured with reference to the '0 min' sample. All experiments were performed in triplicates.

Metabolite Identification. To investigate the metabolites formed by rCYP3A4 and rCYP3A5, dronedarone (20 μM) was incubated with 100 pmol/mL of each supersome, NADPH regenerating system and 100 mM potassium phosphate buffer (pH 7.4) at 37°C. After a 0 or 60-min incubation period, the reaction was terminated and the samples were processed as described above. The '0 min' sample served as the blank control. Metabolite identification was carried out using UPLC/QTOF/MS system.

Time-, Concentration-, and NADPH-Dependent Inactivation of CYP3A4. Two probe substrates of CYP3A4, testosterone and midazolam, were tested in the experiments. Incubation experiments (n=3) were performed in 96-well plates. Primary incubation mixtures consisting of 20 pmol/mL rCYP3A4, 100 mM potassium phosphate buffer (pH 7.4), NADPH B and dronedarone were pre-incubated at 37°C for 5 min. The concentration levels of dronedarone used in the testosterone assay were 0, 0.25, 0.5, 1, 2, 3, 4, 5, and 50 μM while a single concentration level of 50 μM was used for the midazolam assay. To initiate the reactions, 5 μl of NADPH A was added to the mixture. The final primary incubation mixture had a total volume of 100 μL and contained < 1% v/v organic solvent. At 0, 3, 8, 15, 22, and 30 min after the addition of NADPH A, aliquots of the primary incubation mixture were transferred to the secondary incubation mixture containing 200 μM testosterone or 25 μM midazolam, NADPH regeneration system, and 100 mM potassium phosphate buffer (pH 7.4). For the testosterone assay where 0.25, 0.5, 1, 2, 3, 4, 5 μM of dronedarone was used, 5 μL of the primary incubation mixture was transferred to 95 μL of secondary incubation mixture, resulting in a 20× dilution. For the midazolam assay and testosterone assay where 50 μM of dronedarone was used, 10

Molecular Pharmacology Fast Forward. Published on October 21, 2015 as DOI: 10.1124/mol.115.100891
This article has not been copyedited and formatted. The final version may differ from this version.

μL of the primary incubation mixture was transferred to 90 μL of secondary incubation mixture, effecting a 10× dilution. The secondary reaction mixture was incubated for another 10 min at 37°C before an 80-μL aliquot was removed and quenched with an equal volume of ice-cold ACN containing 2 μM prednisolone (IS for testosterone assay) or 0.02 μM carbamazepine (IS for midazolam assay). The quenched samples were centrifuged at 3220 *g* at 4°C for 30 min, and the supernatants were removed for the respective determination of either 6β-hydroxytestosterone or 1'-hydroxymidazolam by LC/MS/MS. The experiment was also performed with erythromycin and ketoconazole that are known mechanism-based inactivator and competitive inhibitor of CYP3A4 respectively. Negative control was performed by replacing 5 μL NADPH A with 100 mM potassium phosphate buffer (pH 7.4). The inactivation assay was repeated by testing NDBD as the inactivator.

To determine the time-, concentration-, and NADPH-dependent activity in the CYP3A4 inactivation assays, the mean of triplicate analyses was used to calculate the natural log of percentage probe substrate activity remaining normalized to 0 min against pre-incubation time. The data was fitted to linear regression and the observed first-order inactivation rate constant, k_{obs}, was determined. Kinetic parameters, K_i and k_{Inact}, were determined by using the Kitz-Wilson plot (Kitz and Wilson, 1962) to calculate the potency of inactivation (k_{inact}/K_i). The graphs were plotted using GraphPad Prism 4.0 (San Diego, CA, USA).

Time-, Concentration-, and NADPH-Dependent Inactivation of CYP3A5. To investigate the potential of suicide inactivation of CYP3A5 by dronedarone and NDBD, rCYP3A5 (20 pmol/mL) was used in place of rCYP3A4 in the two-step incubation scheme described above. 0, 0.25, 0.5, 2.5, 5, 10, 15, 25, and 50 μM dronedarone or NDBD were used for the testosterone assay while 50 μM of each compound was used for the midazolam assay. Both testosterone and midazolam assays were performed using 10× dilution by transferring 10 μL of the primary incubation mixture to 90 μL of secondary incubation mixture. The kinetics parameters were determined as previously described.

Molecular Pharmacology Fast Forward. Published on October 21, 2015 as DOI: 10.1124/mol.115.100891
This article has not been copyedited and formatted. The final version may differ from this version.

Partition Ratio. The partition ratio, defined as the number of inactivator molecules required to completely inactivate the enzyme, was estimated based on the following experiments. Primary incubations (n=3) comprising 100 pmol/mL rCYP3A4, NADPH B, dronedarone (0.5, 2.5, 5, 10, 12.5, 25 μM) or NDBD (0.25, 0.5, 1, 2, 3, 4, 5 μM), and 100 mM potassium phosphate buffer (pH=7.4) were prepared. After pre-incubation at 37 °C for 5 min, the reaction mixtures were initiated by addition of NADPH A and incubated at 37°C for another 45 min, allowing the inactivation to go to completion. Aliquots were then transferred to the secondary incubation mixture with 20× dilution, and assayed for residue enzyme activity as described above for rCYP3A4. The experiment was repeated for dronedarone and NDBD (0, 0.25, 0.5, 2.5, 5, 10, 15, 25 μM) using rCYP3A5 with 10× dilution. To estimate the partition ratio, the percentage of residual enzymatic activity was plotted against the function of the molar ratios of each test inactivator. The turnover number (partition ratio + 1) was extrapolated from the intercept of the linear regression line plotted at lower ratios and the straight line plotted at the higher ratios, to the x-axis. The partition ratio was in turn back calculated from the turnover number by a subtraction of 1.

Substrate Protection. Excess testosterone [in 1:8 ratio of dronedarone (or NDBD) to testosterone] was added to the primary incubation mixture (n=3) containing dronedarone or NDBD (5 μM for rCYP3A4 assay, 25 μM for rCYP3A5 assay), 20 pmol/mL rCYP3A4 or rCYP3A5, NADPH B, and 100 mM potassium phosphate buffer. The reaction was initiated by addition of NADPH A after pre-incubation for 5 min at 37 °C. Aliquots were then transferred to the secondary incubation mixture and assayed for residual enzyme activity as described in the time-dependent inhibition experiment for CYP3A4 and CYP3A5 respectively. Negative controls were prepared without both testosterone and dronedarone or NDBD, or only without testosterone in the primary incubation mixture.

Reversibility of Inactivation. The reversibility of enzyme inactivation was investigated by oxidation with potassium ferricyanide based on a method reported previously (Watanabe et al., 2007). Three sequential incubations were performed, including: primary 0- or 30-min incubation with or without dronedarone/NDBD, secondary 10-min incubation with or without potassium ferricyanide, and

Molecular Pharmacology Fast Forward. Published on October 21, 2015 as DOI: 10.1124/mol.115.100891
This article has not been copyedited and formatted. The final version may differ from this version.

tertiary 10-min incubation with testosterone. The primary incubation solutions consisted of rCYP3A4 or rCYP3A5 (20 pmol/mL), NADPH B, 100 mM potassium phosphate buffer (pH 7.4) and with or without 50 µM dronedarone/ NDBD. After adding NADPH A and incubating for 0 or 30 min at 37°C, 40 µL of each primary incubation was added to 40 µL of secondary incubation containing 100 mM potassium phosphate buffer (pH 7.4) with or without 2 mM potassium ferricyanide. After 10 min incubation, each secondary reaction mixture was diluted 5-fold with the tertiary incubation, which contained 200 µM testosterone, NADPH regeneration system, and 100 mM potassium phosphate buffer (pH 7.4). After 10 min incubation, the reaction mixture was assayed for residual enzyme activity as described in the time-dependent inhibition experiment. The percentage of metabolic activity (% control $_{(0\text{min})}$ and % control $_{(30\text{min})}$) was calculated for each sample after a 0- or 30-min preincubation with dronedarone/NDBD and compared with each control sample without dronedarone/NDBD as follows:

$$\%\ \text{control}_{(0\,\text{min})} = \frac{v_{(0\ min,+\ inhibitor)}}{v_{(0\ min,-\ inhibitor)}} \times 100$$

$$\%\ \text{control}_{(30\,\text{min})} = \frac{v_{(30\ min,+\ inhibitor)}}{v_{(30\ min,-\ inhibitor)}} \times 100$$

V is the residual enzyme activity. Using the above values, the percentage of the enzymatic activity remaining (% remaining) after the 30-min preincubation relative to the 0-min preincubation was calculated as follows:

$$\%\ \text{remaining} = \frac{\%\ \text{of control}_{(30\ \text{min})}}{\%\ \text{of control}_{(0\ \text{min})}} \times 100$$

Spectral Difference Scanning. rCYP3A4 or rCYP3A5 (500 pmol/mL), NADPH B, 50 µM dronedarone or NDBD, and 100 mM potassium phosphate buffer (pH 7.4) were pre-incubated at 37°C for 5 min. The reaction was initiated with the addition of NADPH A. The final mixture had a total volume of 200 µL and contained < 1% v/v organic solvent. The sample mixture was immediately scanned from 400 to 500 nm over 45 min at 37°C using an Infinite M200 Tecan microplate reader (Tecan Group Ltd, Männedorf, Switzerland). The spectral differences were obtained by comparing the signals derived from the sample and reference wells which contained the enzyme, substrate vehicle,

Molecular Pharmacology Fast Forward. Published on October 21, 2015 as DOI: 10.1124/mol.115.100891
This article has not been copyedited and formatted. The final version may differ from this version.

and NADPH. The positive control was prepared using 10 μM verapamil, a known inactivator that forms MI complex with CYP3A4. The extent of MI complex formation was also tracked by measuring absorbance difference between 454 nm and 490 nm.

GSH Trapping. Incubation containing rCYP3A4 or rCYP3A5 (50 pmol/mL), NADPH B, 50 μM test compounds (including dronedarone, NDBD and desulfonated dronedarone), 100 mM potassium phosphate buffer (pH 7.4) and 50 mM GSH were preincubated at 37°C for 5 min. The reaction was initiated by the addition of NADPH A. The total volume of the incubation mixture was 500 μL. After incubating for 60 min, 500 μL of ice-cold ACN was added to quench the reaction. The mixture was centrifuged at 14,000 g for 15 min at 4°C. The supernatant was transferred to a clean microtube and dried under a gentle flow of nitrogen gas (TurboVap LV; Caliper Life Science, Hopkinton, MA). The residue was reconstituted with 60 μL of ACN-water mixture (3:7, v/v), vortex-mixed, and centrifuged at 14,000 g for 15 min at 4 °C. The supernatant was removed for LC/MS/MS analysis. Negative controls were prepared by exclusion of test compounds in the incubation mixture. The chemical synthesis of desulfonated dronedarone is described in the supplementary data.

Measurement of Residual CYP450 Activity. Samples were analyzed using an Agilent 1290 Infinity ultra-high pressure liquid chromatography (UHPLC) (Agilent Technologies Inc., Santa Clara, CA, USA) interfaced with the AB SCIEX QTRAP® 5500 tandem mass spectrometry (MS/MS) system (AB SCIEX, Framingham, MA, USA). The ACQUITY UPLC BEH C_{18}, 1.7 μM, 2.1 × 50 mm column (Waters, Mildord, MA, USA) was used for chromatographic separation. The aqueous mobile phase (A) was 0.1% formic acid in water while the organic mobile phase (B) consisted of 0.1% formic acid in ACN. Mobile phases were delivered at a flow rate of 0.6 mL/min. The column and sample temperatures were maintained at 45°C and 4°C respectively. Gradient elution was first carried out from 20% to 95% of B in 1.40 min. This was subsequently followed by isocratic elution at 95% B for a further 0.59 min before reducing its percentage from 95% to 20% and maintaining it at 20% for another 0.50 min. The source-dependent MS parameters were as follows: Ion Spray (IS) spray voltage = 5000 V; source temperature = 600°C; curtain gas (CUR) = 20 psi; GS1 and GS2 = 65 and 45 psi

Molecular Pharmacology Fast Forward. Published on October 21, 2015 as DOI: 10.1124/mol.115.100891
This article has not been copyedited and formatted. The final version may differ from this version.

respectively. The compound-dependent MS parameters are presented in Table 1. Chromatographic peak integration was performed using the Analyst Software. All graphs were plotted using Prism version 5 (GraphPad Software, San Diego, CA).

Metabolite Identification. A Waters AQUITY UPLC system (Waters, Milford, MA, USA) coupled to a quadrupole time-of-flight mass spectrometer (QTOF/MS, Q-Tof Premier™, Waters, UK) was operated in a positive and MS/MS mode with electrospray ionization. Dronedarone and its metabolites were separated on a Waters UPLC BEH C_{18} column (1.7 µM, 2.1 × 100 mm) with 0.2% acetic acid and 5 mM ammonium acetate (solvent A) in water and 0.2% acetic acid in ACN (solvent B). The column heater and sample manager were kept at 45°C and 4°C respectively. The gradient elution comprised a linear gradient of 20 to 70% B over 0-10 min. The optimized MS conditions were as follows: capillary voltage, 3500 V; sampling cone, 40 V; source temperature, 100 °C; desolvation temperature, 350 °C; cone gas flow, 0 L/h; desolvation gas flow, 300 L/h; collision energy, 25 eV; MCP detector voltage, 1900 V; pusher voltage, 905 V; pusher voltage offset, -0.8 V; and puller voltage, 610 V. The acquisition rate was set to 1 s, with a 0.1 s inter-scan delay. The MS was calibrated across the mass range 100-1500 Da using a solution of sodium formate. All analyses were acquired using the LockSpray™ to ensure accuracy and reproducibility. Leucine-enkephalin was used as the lock mass (*m/z* 556.2771) at a concentration of 2 ng/µL, and flow rate of 3 µL/min. The LockSpray™ was operated at a reference scan frequency, reference cone voltage and collision energy of 10 s, 30 V and 18 V, respectively.

Detection of GSH Adducts. GSH adducts of potential electrophilic reactive metabolites were analyzed using the same UPLC/QTRAP/MS system as described above. Chromatographic separation was performed on a Waters ACQUITY UPLC BEH C_{18} column (1.7 µM, 100 × 2.1 mm). The mobile phases consisted of 0.1% formic acid in water and 0.1% formic acid in ACN and delivered at a flow rate of 0.45 mL/min. The column and sample temperatures were maintained at 45°C and 4°C respectively. The elution gradient was as follows: linear gradient 5 to 60% (0 – 6.25 min), isocratic at 95% (6.26 – 7.00 min), and isocratic at 5% B (7.01 – 8.00 min). Information dependent acquisition

Molecular Pharmacology Fast Forward. Published on October 21, 2015 as DOI: 10.1124/mol.115.100891
This article has not been copyedited and formatted. The final version may differ from this version.

(IDA) experiment was performed to detect GSH conjugates, including precursor ion (PI) 272 (-) with enhanced product ion (EPI) scan. The compound-dependent MS parameters were: DP = 168 V; EP = 10 V; CE = 45 V; CXP = 10 V. The source-dependent parameters were as follows: CUR = 20 psi; CAD = high; IS = 5000 V; source temperature = 650°C; GS1 = 45 psi; GS2 = 60 psi.

For accurate mass measurement of the GSH adducts, the same samples were analysed using Ultimate 3000 nanoLC system (Dionex, Thermo Fisher Scientific, MA, USA) coupled to AB Sciex 5600 TripleTOF mass spectrometer (TripleTOF/MS, AB Sciex, Framingham, MA, USA). A 15 cm × 75 µm i.d. packed with Acclaim PepMap RSLC C_{18} column was used (Dionex, Thermo Fisher Scientific, MA, USA). This column was connected to a spray tip (New Objectives, Woburn, MA), which was directly coupled with the nano-spray interface into TripleTOF/MS. Samples were loaded onto a trap column (Acclaim PepMap 100 C_{18}, 2 cm x 75 µm i.d., Dionex, Thermo Fisher Scientific, MA, USA) at a flow rate of 5 µL/min. After a 3 min wash with loading buffer (2/98 v/v of ACN/water with 0.1% formic acid), the system was switched into line with the C_{18} analytical capillary column. A step linear gradient of mobile phase B (2/98 v/v of water/ACN with 0.1% formic acid) from 5% to 7% for 3-min, 7%-60% for 11 min, and lastly, 60%-95% over 1 min at flow rate of 300 nL/min was utilized for the analysis. Other instrumentation settings of TripleTOF/MS were as follows: ionspray voltage floating (ISVF) = 2400 V; CUR = 30 psi; GS1 = 12 psi; interface heater temperature (IHT) = 125°C, DP = 100 V, nebuliser current (NC) = 3 for nitrogen gas. Data was acquired using product ion MS2 scan and Analyst TF 1.7 software (AB Sciex, Framingham, MA, USA). The collision energy (CE) was set to 44 V with collision energy spread (CES) of 5 V.

Molecular Pharmacology Fast Forward. Published on October 21, 2015 as DOI: 10.1124/mol.115.100891
This article has not been copyedited and formatted. The final version may differ from this version.

RESULTS

Metabolic Stability and Enzyme Kinetics. For the metabolic stability assay, the percentage of dronedarone remaining in the HLM reaction mixture decreased as the incubation time progressed from 0 to 60 min. The calculated *in vitro* metabolism half-life ($t_{1/2}$) and elimination rate constant of dronedarone were 15.42 min and 0.045 min^{-1} respectively (Fig. 2A). The metabolism of dronedarone to NDBD was found to be linear from 0 to 30 min. Using an incubation time of 15 min, our results showed that the metabolism of dronedarone to NDBD, follows Michaelis-Menten kinetics. The calculated K_m was 8.83 μM while V_{max} was 53.4 nmol min^{-1} mg^{-1} proteins (Fig. 2B).

CYP450 Reaction Phenotyping. Our results showed that dronedarone was extensively metabolized by CYP3A4 (Fig. 3A) and CYP3A5 (Fig. 3B), with $t_{1/2}$ of 5.38 and 13.31 min, respectively. On the other hand, CYP2D6 (Fig. 3C) and CYP2C19 (Fig. 3D) metabolize dronedarone at a slower rate, with $t_{1/2}$ of 33.43 min and >60 min, respectively. Finally, our results confirmed that dronedarone was minimally metabolized by CYP2C8, CYP2C9, CYP2E1 and CYP1A2 (data not shown).

Metabolite Identification. A total of 14 metabolites were identified from the incubation of dronedarone with rCYP3A4 or rCYP3A5. The detailed information, including the retention time (RT), proposed formula, measured *m/z* ratio of the MH^+ ions, and characteristic product ions, are summarized in Table 2. The most abundant metabolite M1 with an *m/z* reduction of 56 (corresponding to a loss of a C_4H_8 functional group) compared to the parent ion, was confirmed to be NDBD using standard. Five metabolites (M2-1 to M2-5) were found to have an *m/z* reduction of 40, and are likely the secondary oxidised metabolites of dronedarone after undergoing *N*-desbutylation. When compared to the parent drug, seven of the metabolites (M3-1 to M3-7) exhibited an increase in *m/z* of 16, which are possibly associated with hydroxylation of dronedarone. M4 demonstrated an increase in *m/z* of 32 and is possibly a result of the dioxidation of dronedarone.

Molecular Pharmacology Fast Forward. Published on October 21, 2015 as DOI: 10.1124/mol.115.100891
This article has not been copyedited and formatted. The final version may differ from this version.

Time-, Concentration-, and NADPH-Dependent Inactivation of CYP3A4 and CYP3A5. Dronedarone inactivated CYP3A4 in a time- and NADPH-dependent manner with testosterone as probe substrate (Supplemental Figure 1A). As shown in Figures 4A and 4B, the inactivation of CYP3A4 by dronedarone and NDBD was also concentration-dependent. The observed rate of inactivation (k_{obs}) calculated from various concentration levels of dronedarone and NDBD followed saturation kinetics that approached a maximum rate of inactivation (Fig. 4C and Fig. 4D). The K_I and k_{Inact} values for the inactivation of CYP3A4 by dronedarone were determined to be 0.873 μM and 0.039 min^{-1}, respectively, which in turn yielded a k_{Inact}/K_I ratio of 0.0445 $min^{-1}\cdot\mu M^{-1}$ (Fig. 4C). The time required for half of the enzyme molecules to be inactivated ($t_{1/2}$) was 17.8 min. In a similar fashion, as shown in Figure 4D, NDBD inactivated CYP3A4 with K_I and k_{Inact} values of 6.242 μM and 0.099 min^{-1} respectively and a k_{Inact}/K_I ratio of 0.0158 $min^{-1}\cdot\mu M^{-1}$. The inactivation $t_{1/2}$ was 7.0 min. To further assess the inactivation of CYP3A4 by dronedarone and NDBD, another well characterized CYP3A4 probe substrate, midazolam was also tested. Time- and NADPH- dependent inactivation of CYP3A4 were also observed when midazolam was used as the probe substrate for both dronedarone (Supplemental Figure 1C) and NDBD (Supplemental Figure 1D). However, a lower potency of inactivation of CYP3A4 was observed as compared to when testosterone was used as the probe substrate. The positive control, erythromycin (a known mechanism-based inactivator of CYP3A4), demonstrated time-, concentration-, and NADPH-dependent inactivation of CYP3A4 (Supplemental Figure 1E). On the other hand, the negative control, ketoconazole (a competitive inhibitor of CYP3A4), did not yield time-dependency of CYP3A4 inhibition (Supplemental Figure 1F).

Inhibition of CYP3A5 by dronedarone (Supplemental Figure 2A) and NDBD (Supplemental Figure 2B) demonstrated time-, concentration-, and NADPH-dependence with testosterone as substrate. As shown in Supplemental Figure 2C, the K_I , k_{Inact} and $t_{1/2}$ values for dronedarone were determined to be 2.186 μM, 0.0056 min^{-1} and 123.1 min, respectively. On the other hand, the K_I, k_{Inact} and $t_{1/2}$ values for NDBD were 5.445 μM, 0.0563 min^{-1} and 12.3 min, respectively (Supplemental Figure 2D). Time- and NADPH-dependent CYP3A5 inactivation by dronedarone was also observed when midazolam was used as the probe substrate. Similarly, the potency of inactivation was lower (data not shown).

Molecular Pharmacology Fast Forward. Published on October 21, 2015 as DOI: 10.1124/mol.115.100891
This article has not been copyedited and formatted. The final version may differ from this version.

Partition Ratio. The partition ratios of dronedarone and NDBD with regards to the inactivation of CYP3A4 were 51.1 and 35.3 respectively (Fig. 5A and Fig. 5B). As for the inactivation of CYP3A5, the respective partition ratios were 32.2 and 36.6 (Supplemental Figure 3A and Supplemental Figure 3B).

Substrate Protection. Testosterone, an alternate substrate of CYP3A4 and CYP3A5, was included in the primary incubations along with dronedarone or NDBD. As shown in Figures 5C and 5D, the inactivation of CYP3A4 by both dronedarone and NDBD was protected in the presence of 8-fold excess testosterone. Similar observations were made for the substrate protection of CYP3A5 inactivation (Supplemental Figure 3C and Supplemental Figure 3D).

Reversibility of Inactivation. To investigate whether the inactivation of CYP3A4 and CYP3A5 by dronedarone and NDBD is quasi-irreversible or irreversible, oxidation with potassium ferricyanide was performed based on a method reported previously (Watanabe et al., 2007). Upon oxidation using potassium ferricyanide, the metabolic activity of CYP3A4 and CYP3A5 was restored by 10.9% and 19.4% post-inactivation by dronedarone, and 22.6% and 32% post-inactivation by NDBD (Table 3).

Spectral Difference Scanning. Spectral difference scanning experiments were performed to investigate whether the inactivation of CYP3A4 and CYP3A5 by dronedarone and NDBD occurred via the formation of MI complex. A clear peak at 448 to 458 was observed when verapamil (forms a MI complex with CYP3A4) (Ma et al., 2000) was incubated with rCYP3A4 (Supplemental Figure 4A), but not when lapatinib (a known mechanism-based inactivator of CYP3A5 that does not form a MI complex) (Chan et al., 2012) was incubated with rCYP3A5 (Supplemental Figure 4B). When spectral differences were obtained by scanning from 400 to 500 nm for 45 min, both dronedarone and NDBD showed an observable peak in the Soret region when incubated with both CYP3A4 and CYP3A5 (Fig. 6A-D). Absorbance difference between 454 nm and isobestic point 490 nm tracks the extent of MI complex formation. MI complexes formed between CYP3A4 (Fig. 6E) and CYP3A5

Molecular Pharmacology Fast Forward. Published on October 21, 2015 as DOI: 10.1124/mol.115.100891
This article has not been copyedited and formatted. The final version may differ from this version.

(Fig. 6F) with dronedarone and NDBD were observed to accumulate over time and reach a maximum after approximately 40 min of incubation. Similarly, positive control performed with verapamil also showed an accumulation of MI complex formation (Supplemental Figure 4C).

GSH Trapping. GSH Trapping assay was performed to screen for potential electrophilic reactive metabolites that cause MBI of CYP3A4 and CYP3A5 via covalent binding. One suggestive GSH adduct with *m/z* 800 (RT 5.04 min) was detected in the incubation of dronedarone with both rCYP3A4 (Supplemental Figure 5A) and rCYP3A5 (data not shown), based on the precursor ion scan experiments performed at *m/z* 272 in the ESI negative mode. The EPI spectrum yielded a product ion at *m/z* 479, corresponding to the desulfonated metabolite of dronedarone. This was further confirmed by the detection of the same GSH adduct in the incubation of chemically synthesized desulfonated dronedarone with rCYP3A4/5 and GSH. For NDBD, a potential GSH adduct with *m/z* 744 (RT 4.42 min) was found in the incubation with rCYP3A4 (Supplemental Figure 5B) and rCYP3A5 (data not shown). Similarly, a product ion at *m/z* 423 corresponding to the desulfonated metabolite of NDBD was detected (Supplemental Figure 5B). To further confirm the identity of the potential GSH adduct, accurate mass measurement was performed using TripleTOF/MS. The proposed chemical formulae, experimental accurate *m/z*, theoretical exact *m/z* and mass accuracy (ppm) associated with the parent and product ions of dronedarone-GSH adduct are summarized in Table 4. Our data suggested the GSH adducts were formed via covalent binding with the oxime metabolites derived from both desulfonated dronedarone and desulfonated NDBD. The MS/MS spectrum (Fig. 7) confirmed the accurate mass fragmentation patterns of the oxime metabolite-GSH adduct derived from dronedarone.

Molecular Pharmacology Fast Forward. Published on October 21, 2015 as DOI: 10.1124/mol.115.100891
This article has not been copyedited and formatted. The final version may differ from this version.

Discussion

Dronedarone causes DDIs and liver toxicity but the mechanism is currently unknown. The present study provides evidences for the first time that demonstrate the inactivation of CYP3A4 and CYP3A5 by dronedarone and its main metabolite NDBD.

Our *in vitro* assay using rCYP450 confirmed that dronedarone is extensively metabolized by CYP3A4 and CYP3A5, in agreement with a previous report (Klieber et al., 2014). Additionally, we found that while CYP2D6 and CYP2C19 contribute to the metabolism of dronedarone, CYP2C8, CYP2C9, CYP1A2 and CYP2E1 do not metabolize dronedarone. Therefore, the subsequent metabolite identification and CYP450 inactivation studies were focused mainly on CYP3A4 and CYP3A5.

Dronedarone was found to be extensively metabolized to a number of metabolites by CYP3A4 and CYP3A5, mainly through *N*-desbutylation and hydroxylation. Our *in vitro* observation that NDBD is the main metabolite of dronedarone is consistent with clinical data that the plasma systemic exposure of NDBD is approximately half that of its parent drug following oral administration (USFDA, 2008). Notably, NDBD is pharmacologically active *in vivo* (USFDA, 2008) and is further oxidized by CYP3A4 (Klieber et al., 2014).

As hypothesized, our results demonstrated that both dronedarone and NDBD inactivate CYP3A4 and CYP3A5 in a time-, concentration-, and NADPH-dependent manner. To estimate and appreciate the inactivation potency of dronedarone, k_{Inact}/K_I ratios were calculated and compared with that of known inactivators such as clarithromycin, erythromycin and amprenavir that inactivate CYP3A4 via the formation of MI complex (Table 5). Based on the inactivation of CYP3A4-mediated testosterone-6β-hydroxylation, dronedarone and NDBD were found to have lower potencies as compared to potent inactivator such as amprenavir (Ernest et al., 2005), but comparable inactivation potencies as compared to moderate inactivators such as clarithromycin and erythromycin (Polasek and Miners, 2006). In other words, the inactivation of CYP3A4 by dronedarone and NDBD is clinically important. Notably, both dronedarone and NDBD demonstrated greater inactivation potencies against CYP3A4

Molecular Pharmacology Fast Forward. Published on October 21, 2015 as DOI: 10.1124/mol.115.100891
This article has not been copyedited and formatted. The final version may differ from this version.

as compared to CYP3A5. This underscores the important difference between the two CYP3A isoforms in terms of inactivation characteristics.

The efficiency of CYP450 inactivation is estimated by its partition ratio, which is the number of inactivator molecules required to completely inactivate the enzyme. In theory, a lower partition ratio implies a more efficient CP450 inactivation. The partition ratio for the inactivation of CYP3A4 by dronedarone is higher than that of NDBD, suggesting the parent drug is less efficient in inactivating the enzyme as compared to its main metabolite. This finding supports our hypothesis as NDBD is possibly the intermediate metabolite leading to the formation of the reactive intermediates. On the other hand, dronedarone and NDBD displayed similar partition ratios against CYP3A5, suggesting equal efficiency in its inactivation. The less distinctive partition ratios in the case of CYP3A5 might be due to the overall lower potency of dronedarone and NDBD in inactivating this CYP3A isoform (Table 5). Co-incubation with another specific CYP3A substrate, testosterone, protected both CYP3A4 and CYP3A5 from inactivation by dronedarone and NDBD, further confirming that inactivation occurred within the active site of the enzymes.

The substrate specificity of CYP3A is relatively low due to its large active site (Fowler and Zhang, 2008). Research has shown that there are multiple binding modes of substrates within CYP3A (Ekins et al., 2003). In the present study, the inactivation of CYP3A4 and CYP3A5 by dronedarone and NDBD using midazolam as a probe substrate was also investigated. Compared to the inactivation of testosterone 6β-hydroxylation, inactivation of midazolam 1'-hydroxylation by dronedarone and NDBD was less significant. This demonstrates the inactivation of the two CYP3A isoforms by dronedarone and NDBD is substrate-specific. As reported before, lapatinib also yields site-specific MBI of CYP3A5 (Chan et al., 2012). As the potential clinical DDIs arising from the inactivation of CYP3A4 and CYP3A5 by dronedarone and NDBD are substrate-specific, prudent clinical interpretation needs to be exercised.

Molecular Pharmacology Fast Forward. Published on October 21, 2015 as DOI: 10.1124/mol.115.100891
This article has not been copyedited and formatted. The final version may differ from this version.

MI complex forms a Soret peak at approximately 448 to 455 nm, due to the presence of a coordinate bond formed between the reactive intermediate and ferrous iron of the CYP450 heme group(Buening and Franklin, 1976; Franklin, 1972; Mansuy et al., 1976). To test our hypothesis that dronedarone and NDBD form MI complex with CYP3A, spectral difference scanning experiment was performed. The observance of Soret peaks with maximal absorbance at ~454 nm confirmed that both dronedarone and NDBD inactivated CYP3A4 and CYP3A5 via the formation of MI complexes.

The reaction sequence to MI complex formation from tertiary alkylamine has been proposed by Hanson et al. (Hanson et al., 2010). *N*-dealkylation occurs to yield a secondary amine followed by two potential pathways, namely: (1) hydroxylation of the secondary amine leading to the nitroso intermediate or (2) a second *N*-dealkylation forms a primary amine ultimately leading to the same nitroso intermediate. By comparing the inactivation rate constant k_{Inact}, the MI complex formation by NDBD is more efficient than dronedarone against both CYP3A4 and CYP3A5. This implies that *N*-desbutylation of dronedarone to NDBD is possibly the first bioactivation step towards the formation of MI complex. Interestingly, five metabolites (M2-1 to M2-5) were identified to be hydroxylated NDBD as confirmed using accurate mass spectrometry (Table 2). Based on the evidences, we propose the formation MI complex between dronedarone and CYP3A is mediated through hydroxylation of the amino group of the NDBD followed by the subsequent formation of a nitroso intermediate (Fig. 8).

Quasi-irreversible MI complex can be dissociated by oxidation with potassium ferricyanide(Buening and Franklin, 1976). This is followed by the recovery of CYP450 enzymatic activity. In contrast, for MBI, the inactivated CYP450 enzymatic activity is irreversible and cannot be restored. Based on a published criterion (Watanabe et al., 2007), CYP3A enzymatic activity inactivated after a 30-min preincubation with quasi-irreversible inactivators can be restored by more than 20% with the addition of potassium ferricyanide. For irreversible inactivation, the recovery of enzyme activity is less than 20%. The metabolic activity of inactivated CYP3A4 and CYP3A5 was restored by less than 20% for dronedarone, and more than 20% for NDBD after the addition of potassium ferricyanide (Table 3).

Molecular Pharmacology Fast Forward. Published on October 21, 2015 as DOI: 10.1124/mol.115.100891
This article has not been copyedited and formatted. The final version may differ from this version.

Our findings hinted the possibility of an electrophilic reactive metabolite of dronedarone that inactivates CYP3A via an additional irreversible MBI pathway.

Indeed, reactive metabolite-GSH adducts were found for the first time when dronedarone and NDBD were incubated with CYP3A4 and CYP3A5. EPI spectrum suggested that the GSH adduct was formed via the formation of a covalent bond between cysteine thiol of GSH and the electrophilic oxime metabolite derived from desulfonated dronedarone (Fig. 7 and Table 4). Similar observations were made for GSH adducts derived from NDBD and synthesized desulfonated dronedarone. Collectively, our findings confirmed that desulfonation of both dronedarone and NDBD precedes the formation of the oxime metabolites and suggests the latter as the species that inactivate CYP3A4 and CYP3A5 via covalent and irreversible MBI. While the recovery of enzymatic activity was more than 20% after adding potassium ferricyanide to NDBD incubations, one has to consider two key factors before ruling out MBI of CYP3A by NDBD. First, the stipulated criterion (Watanabe et al., 2007) may not be applicable to mixed mode inactivator such as NDBD where it inactivates CYP3A via both MBI and formation of MI complex. Second, the greater recovery of enzymatic activity observed for NDBD (>20%) is supportive of our earlier finding that the MI complex formation by NDBD is more efficient than dronedarone against both CYP3A4 and CYP3A5.

In conclusion, we demonstrated for the first time that dronedarone and NDBD inactivate CYP3A4 and CYP3A5 site-specifically via the formation of both quasi-irreversible MI complexes and quinone oxime-mediated covalent adducts (Fig. 8). With a deeper elucidation of the mechanisms of CYP3A inactivation, our findings fuel new knowledge in understanding clinical DDIs and hepatotoxicity associated with dronedarone. Nevertheless, further clinical or physiological-based pharmacokinetics (PBPK) studies are necessary to confirm the clinical significance of CYP3A inactivation by dronedarone in DDIs. In addition, while our study discovers the potential of dronedarone and NDBD in covalent binding to cellular nucleophiles, further studies need to be performed to elucidate the molecular mechanisms associated with dronedarone-induced hepatotoxicity.

Molecular Pharmacology Fast Forward. Published on October 21, 2015 as DOI: 10.1124/mol.115.100891
This article has not been copyedited and formatted. The final version may differ from this version.

AUTHORSHIP CONTRIBUTIONS

Participated in research design: Hong, Kojodjojo and Chan

Conducted experiments: Hong, Chia, Yeo, Venkatesan and Koh

Contributed new reagents or analytic tools: Chai and Zhou

Performed data analysis: Hong, Chia, Yeo, Venkatesan and Koh

Wrote or contributed to the writing of the manuscript: Hong, Chia, Yeo, Venkatesan and Chan

REFERENCES

Buening MK and Franklin MR (1976) SKF 525-A inhibition, induction, and 452-nm complex formation. *Drug Metab Dispos* **4**(3): 244-255.

Chan ECY, New LS, Chua TB, Yap CW, Ho HK and Nelson SD (2012) Interaction of lapatinib with cytochrome P450 3A5. *Drug Metab Dispos* **40**(7): 1414-1422.

De Ferrari GM and Dusi V (2012) Drug safety evaluation of dronedarone in atrial fibrillation. *Expert Opin Drug Saf* **11**(6): 1023-1045.

Delaforge M, Jaouen M and Mansuy D (1983) Dual effects of macrolide antibiotics on rat liver cytochrome P-450: Induction and formation of metabolite-complexes: A structure-activity relationship. *Biochem Pharmacol* **32**(15): 2309-2318.

Ekins S, Stresser DM and Andrew Williams J (2003) In vitro and pharmacophore insights into CYP3A enzymes. *Trends Pharmacol Sci* **24**(4): 161-166.

Ernest CS, Hall SD and Jones DR (2005) Mechanism-based inactivation of CYP3A by HIV protease inhibitors. *J Pharmacol Exp Ther* **312**(2): 583-591.

Ferrari GMD and Dusi V (2012) Drug safety evaluation of dronedarone in atrial fibrillation. *Expert Opin Drug Saf* **11**(6): 1023-1045.

Fowler S and Zhang H (2008) In vitro evaluation of reversible and irreversible cytochrome P450 inhibition: current status on methodologies and their utility for predicting drug-drug interactions. *AAPS J* **10**(2): 410-424.

Franklin MR (1972) Piperonyl Butoxide Metabolism by Cytochrome P-450: Factors Affecting the Formation and Disappearance of the Metabolite-Cytochrome P-450 Complex. *Xenobiotica* **2**(6): 517-527.

Grimm SW, Einolf HJ, Hall SD, He K, Lim HK, Ling KH, Lu C, Nomeir AA, Seibert E, Skordos KW, Tonn GR, Van Horn R, Wang RW, Wong YN, Yang TJ and Obach RS (2009) The conduct of in vitro studies to address time-dependent inhibition of drug-metabolizing enzymes: a perspective of the pharmaceutical research and manufacturers of America. *Drug Metab Dispos* **37**(7): 1355-1370.

Hanson KL, VandenBrink BM, Babu KN, Allen KE, Nelson WL and Kunze KL (2010) Sequential metabolism of secondary alkyl amines to metabolic-intermediate complexes: opposing roles for the secondary hydroxylamine and primary amine metabolites of desipramine,(s)-fluoxetine, and N-desmethyldiltiazem. *Drug Metab Dispos* **38**(6): 963-972.

Klieber S, Arabeyre-Fabre C, Moliner P, Marti E, Mandray M, Ngo R, Ollier C, Brun P and Fabre G (2014) Identification of metabolic pathways and enzyme systems involved in the in vitro human hepatic metabolism of dronedarone, a potent new oral antiarrhythmic drug. *Pharmacol Res Perspect* **2**(3): doi:10.1002/prp1002.1044.

Ma B, Prueksaritanont T and Lin JH (2000) Drug interactions with calcium channel blockers: possible involvement of metabolite-intermediate complexation with CYP3A. *Drug Metab Dispos* **28**(2): 125-130.

Mansuy D, Beaune P, Chottard J, Bartoli J and Gans P (1976) The nature of the "455 nm absorbing complex" formed during the cytochrome P450 dependent oxidative metabolism of amphetamine. *Biochem Pharmacol* **25**(5): 609-612.

Naccarelli GV, Wolbrette DL, Levin V, Samii S, Banchs JE, Penny-Peterson E and Gonzalez MD (2011) Safety and efficacy of dronedarone in the treatment of atrial fibrillation/flutter. *Clin Med Insights Cardiol* **5**: 103-119.

Ohyama K, Nakajima M, Suzuki M, Shimada N, Yamazaki H and Yokoi T (2000) Inhibitory effects of amiodarone and its N-deethylated metabolite on human cytochrome P450 activities: Prediction of in vivo drug interactions. *Br J Clin Pharmacol* **49**(3): 244-253.

Oyetayo OO, Rogers CE and Hofmann PO (2010) Dronedarone: a new antiarrhythmic agent. *Pharmacotherapy* **30**(9): 904-915.

Pamukcu B and Lip GY (2011) Dronedarone as a new treatment option for atrial fibrillation patients: pharmacokinetics, pharmacodynamics and clinical practice. *Expert Opin Pharmacother* **12**(1): 131-140.

Patel C, Yan G-X and Kowey PR (2009) Dronedarone. *Circulation* **120**(7): 636-644.

Polasek TM, Elliot DJ, Lewis BC and Miners JO (2004) Mechanism-based inactivation of human cytochrome P4502C8 by drugs in vitro. *J Pharmacol Exp Ther* **311**(3): 996-1007.

Polasek TM and Miners JO (2006) Quantitative prediction of macrolide drug-drug interaction potential from in vitro studies using testosterone as the human cytochrome P4503A substrate. *Eur J Clin Pharmacol* **62**(3): 203-208.

Trigo P and Fischer GW (2012) Managing atrial fibrillation in the elderly: critical appraisal of dronedarone. *Clin Interv Aging* **7**: 1-13.

USFDA (2008) Clinical pharmacology and biopharmaceutics reviews. Available at: http://www.accessdata.fda.gov/drugsatfda_docs/nda/2009/022425s000_ClinPharm_P1.pdf.

USFDA (2011) FDA Drug Safety Communication: Severe liver injury associated with the use of dronedarone (marketed as Multaq). Available at: http://www.fda.gov/Drugs/DrugSafety/ucm240011.htm.

Vodovar D, Mongardon N, Moachon L, Arnaout M, Beuzeboc P, Lokiec F, Rezai K and Pène F (2011) Severe docetaxel overdose induced by pharmacokinetic interaction with dronedarone. *J Clin Oncol* **29**(24): e694-e695.

Watanabe A, Nakamura K, Okudaira N, Okazaki O and Sudo K-i (2007) Risk assessment for drug-drug interaction caused by metabolism-based inhibition of CYP3A using automated in vitro assay systems and its application in the early drug discovery process. *Drug Metab Dispos* **35**(7): 1232-1238.

Molecular Pharmacology Fast Forward. Published on October 21, 2015 as DOI: 10.1124/mol.115.100891
This article has not been copyedited and formatted. The final version may differ from this version.

FOOTNOTES:

This work was supported by the Singapore Ministry of Education Tier 1 Funding [Grant R-148-000-193-112] and the National University of Singapore, Department of Pharmacy Final Year Project Funding [Grant R-148-000-003-001].

Molecular Pharmacology Fast Forward. Published on October 21, 2015 as DOI: 10.1124/mol.115.100891
This article has not been copyedited and formatted. The final version may differ from this version.

LEGENDS FOR FIGURES

Fig. 1. Chemical structures of (A) dronedarone, (B) amiodarone and (C) *N*-desbutyl dronedarone (NDBD).

Fig. 2. *In vitro* (A) metabolic stability of dronedarone and (B) enzymatic kinetics of metabolism of dronedarone to *N*-desbutyl dronedarone (NDBD).

Fig. 3. Metabolism of dronedarone by selected recombinant CYP isoforms, namely (A) rCYP3A4, (B) rCYP3A5, (C) rCYP2D6 and (D) rCYP2C19.

Fig. 4. Time- and concentration-dependent inactivation of CYP3A4 by (A) dronedarone and (B) NDBD, using testosterone as probe substrate. Observed inactivation rates (k_{obs}) were used to calculate inactivation kinetic constants, K_I and k_{Inact}, using non-linear regression. The K_I and k_{Inact} values were (C) 0.873 μM and 0.039 min^{-1} for dronedarone, and (D) 6.242 μM and 0.099 min^{-1} for NDBD, respectively. Each point in (A) and (B) represents the mean and S.D. of triplicate experiments.

Fig. 5. Determination of the partition ratios for inactivation of CYP3A4 by (A) dronedarone and (B) NDBD. Substrate protection of CYP3A4 inactivation by (C) dronedarone and (D) NDBD. rCYP3A4 was incubated with dronedarone (■), 1:8 dronedarone/testosterone (▲), and neither dronedarone nor testosterone (●). Each point represents the mean and S.D. of triplicate experiments.

Fig. 6. UV absorbance spectral difference measured over 45 min yielded Soret peak at ~454 nm for rCYP3A4 incubated with (A) dronedarone and (B) NDBD; rCYP3A5 incubated with (C) dronedarone, and (D) NDBD. Comparison of absorbance at reference 454 nm against absorbance at 490 nm demonstrated an increase in the extent of MI complex formation over time for both dronedarone and NDBD incubated with (E) CYP3A4 and (F) CYP3A5.

Fig. 7. Accurate mass spectrum and proposed fragmentation pattern of oxime metabolite-GSH adduct derived from dronedarone.

Fig. 8. Proposed CYP3A4- and CYP3A5-mediated metabolism of dronedarone to its quinone oxime reactive intermediate and nitroso intermediate. * GSH adduction is possible at both carbon 4 (C4) and carbon 6 (C6) positions.

Molecular Pharmacology Fast Forward. Published on October 21, 2015 as DOI: 10.1124/mol.115.100891
This article has not been copyedited and formatted. The final version may differ from this version.

TABLE 1

Optimized compound-dependent MS parameters for LC/MS/MS analysis

Compound	Q1 Mass (Da)	Q3 Mass (Da)	DP (Volts)	EP (Volts)	CE (Volts)	CXP (Volts)
Dronedarone	557	100	80	10	46	7
NDBD	501	114	100	11	41	7
Verapamil	455	165	80	10	34	10
Prednisolone	361	147	160	11	29	9
6β-hydroxytestosterone	305	269	200	7	20	11
Carbamazepine	237	194	160	8	26	12
1'-hydroxymidazolam	342	203	130	13	35	13

Q1 Mass: Parent ion *EP: Entrance potential*

Q3 Mass: Daughter ion *CE: Collision energy*

DP: Declustering potential *CXP: Collision cell exit potential*

TABLE 2

Characteristics of major metabolites identified using accurate mass measurement following incubation of dronedarone with rCYP3A4 and rCYP3A5

Description	Assignment	Retention Time (min)	Measured MH^+ (*m/z*)	Theoretical MH^+ (*m/z*)	Proposed formula	Product ions (*m/z*)
Parent drug	M0	6.11	557.3036	557.3049	$C_{31}H_{45}N_2O_5S^+$	100, 142, 294, 435
N-desbutylation	M1	4.75	501.2437	501.2423	$C_{27}H_{37}N_2O_5S^+$	114, 121, 336, 379
N-desbutylation + Oxidation	M2-1	2.03	517.2367	517.2372	$C_{27}H_{37}N_2O_6S^+$	114, 121, 395, 438
	M2-2	2.14	517.2380	517.2372	$C_{27}H_{37}N_2O_6S^+$	114, 121, 344, 386
	M2-3	2.49	517.2397	517.2372	$C_{27}H_{37}N_2O_6S^+$	114, 121, 386, 459
	M2-4	2.87	517.2385	517.2372	$C_{27}H_{37}N_2O_6S^+$	114, 121, 344, 386
	M2-5	3.87	517.2391	517.2372	$C_{27}H_{37}N_2O_6S^+$	114, 130, 395, 414
Oxidation	M3-1	3.48	573.2984	573.2998	$C_{31}H_{45}N_2O_6S^+$	100, 142, 170, 451
	M3-2	3.90	573.2996	573.2998	$C_{31}H_{45}N_2O_6S^+$	100, 142, 515, 555
	M3-3	4.25	573.2996	573.2998	$C_{31}H_{45}N_2O_6S^+$	100, 142, 451, 555
	M3-4	4.86	573.2901	573.2998	$C_{31}H_{45}N_2O_6S^+$	114, 170, 501
	M3-5	5.04	573.3005	573.2998	$C_{31}H_{45}N_2O_6S^+$	100, 142, 308, 449
	M3-6	5.27	573.3051	573.2998	$C_{31}H_{45}N_2O_6S^+$	100, 142, 451, 493
	M3-7	5.40	573.2938	573.2998	$C_{31}H_{45}N_2O_6S^+$	100, 142, 501, 555
Di-oxidation	M4	2.47	589.2966	589.2948	$C_{31}H_{45}N_2O_7S^+$	100, 170, 467, 545

TABLE 3

Reversibility of inactivation of CYP3A4 and CYP3A5 by dronedarone and NDBD

	System	CYP3A4		CYP3A5	
		%Control (0 min)	%Control (30 min)	%Control (0 min)	%Control (30 min)
Dronedarone	-KFC	36.5 ± 2.2	21.0 ± 4.2	76.5 ± 4.3	56.6 ± 6.8
	+KFC	42.2 ± 5.6	31.9 ± 1.1	84.9 ± 2.0	76.0 ± 5.2
	% Reversed	/	10.9	/	19.4
NDBD	-KFC	49.7 ± 7.6	42.4 ± 3.8	55.5 ± 1.2	28.9 ± 2.4
	+KFC	50.2 ± 4.8	65.0 ± 0.6	73.5 ± 1.5	60.9 ± 1.0
	% Reversed	/	22.6	/	32.0

KFC: Potassium ferricyanide.

TABLE 4

Accurate mass analysis of the parent and product ions of oxime metabolite-GSH adduct derived from dronedarone

Proposed Chemical Formula	***m/z***		**ppm**
	Theoretical	**Experimental**	
$C_{40}H_{58}N_5O_{10}S$	800.3899	800.3886	-1.62
$C_{30}H_{43}N_2O_4S$	527.2938	527.2933	-0.95
$C_{30}H_{39}N_2O_3S$	509.2832	509.2826	-1.18
$C_{30}H_{42}N_2O_3$	479.3268	479.3262	-1.25
$C_{27}H_{35}N_2O_3$	435.2642	435.2639	-0.69
$C_{18}H_{12}NO_5$	322.0710	322.0705	-1.55
$C_{10}H_{14}N_3O_5$	256.0928	256.0929	0.39
$C_8H_9N_2O_3$	181.0607	181.0604	-1.66

TABLE 5

Comparison of enzyme inactivation kinetic constants using testosterone-6β-hydroxylation activity of CYP3A4 and CYP3A5 as indication of residual activity

Drug and Metabolite	**K_I (μM)**		**k_{Inact} (min^{-1})**		**k_{Inact}/K_I ($min^{-1}\cdot mM^{-1}$)**		**$t_{1/2}$ (min)**		**Partition ratio**	
	CYP3A4	**CYP3A5**	**CYP3A4**	**CYP3A5**	**CYP3A4**	**CYP3A5**	**CYP3A4**	**CYP3A5**	**CYP3A4**	**CYP3A5**
Dronedarone	0.87	2.19	0.039	0.0056	44.83	2.56	17.8	123.1	51.1	32.2
NDBD	6.24	5.45	0.099	0.056	15.87	10.28	7.0	12.3	35.3	36.6
Clarithromycin	2.25	ND	0.04	ND	17.78	ND	ND	ND	ND	ND
Erythromycin	0.92	ND	0.058	ND	63.04	ND	ND	ND	ND	ND
Amprenavir	0.26	0.20	0.73	0.35	2808	1750	ND	ND	ND	ND

Figure 1

A

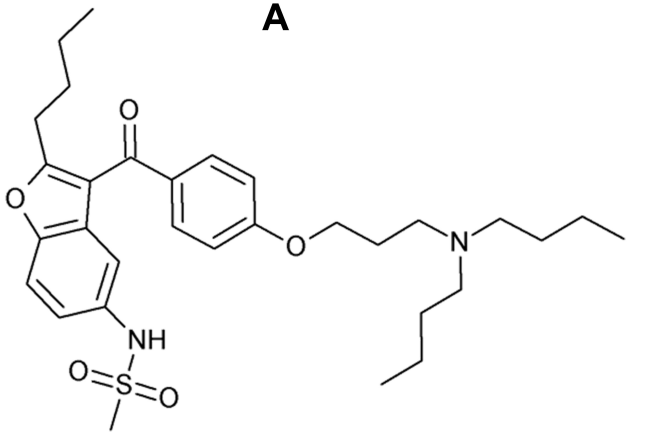

B

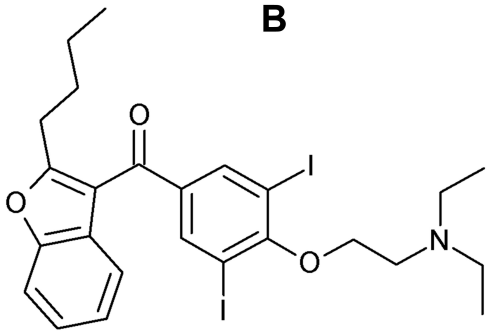

C

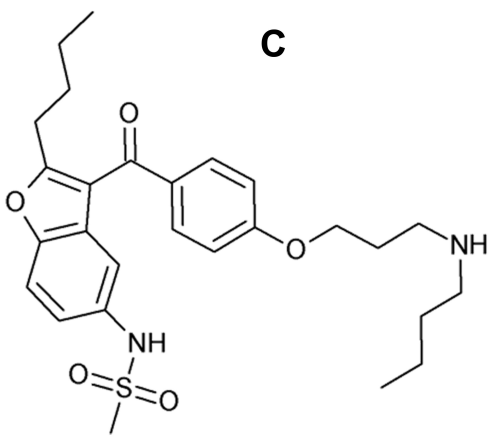

Figure 2

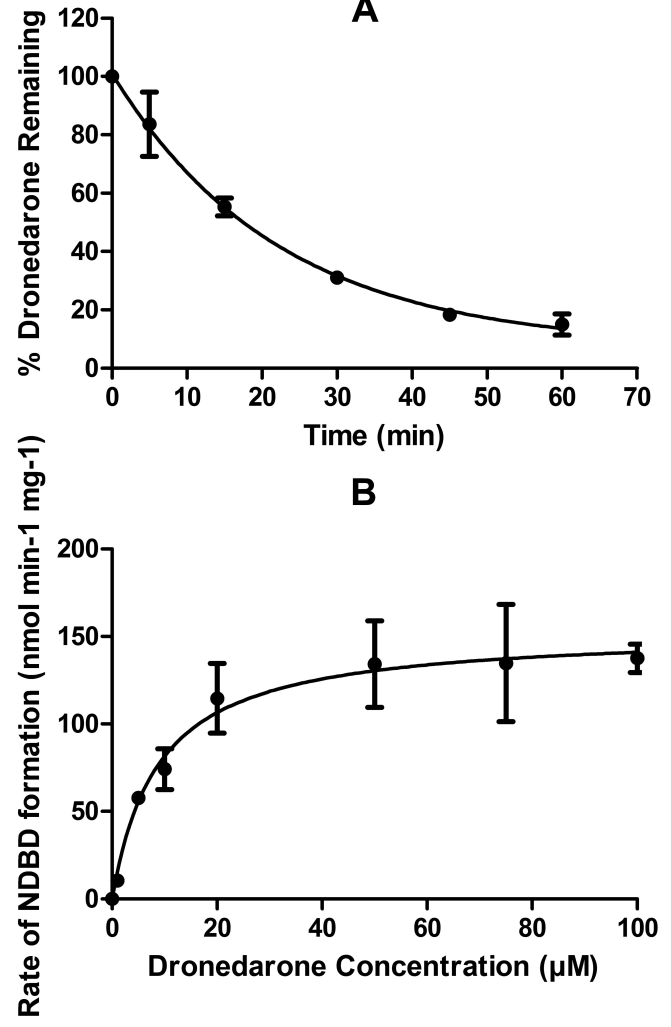
A
% Dronedarone Remaining
120
100
80
60
40
20
0
0
10
20
30
40
50
60
70
Time (min)
B
Rate of NDBD formation (nmol min-1 mg-1)
200
150
100
50
0
0
20
40
60
80
100
Dronedarone Concentration (μM)

Figure 3

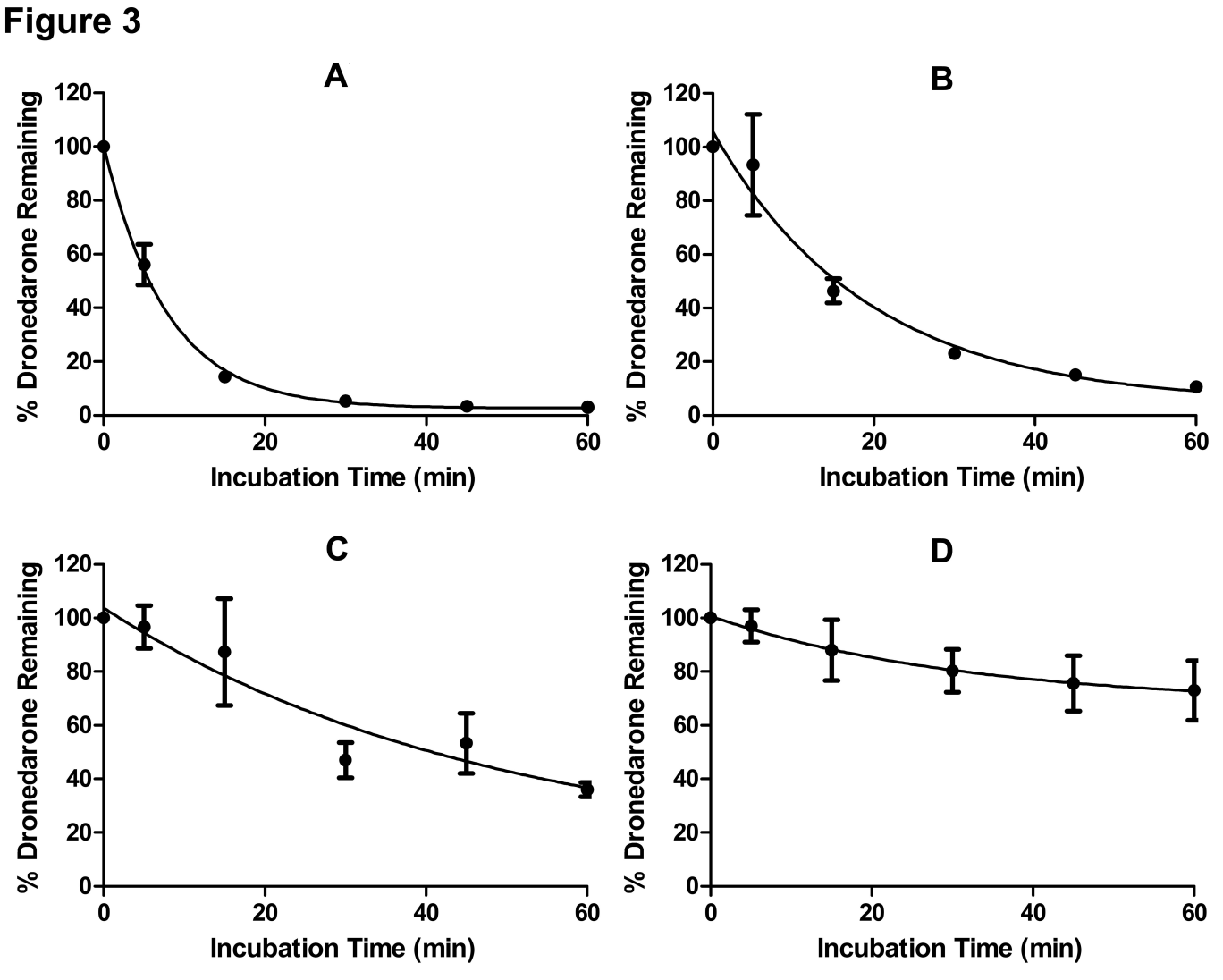
A
B
C
D
% Dronedarone Remaining
Incubation Time (min)
0
20
40
60
80
100
120

Figure 4

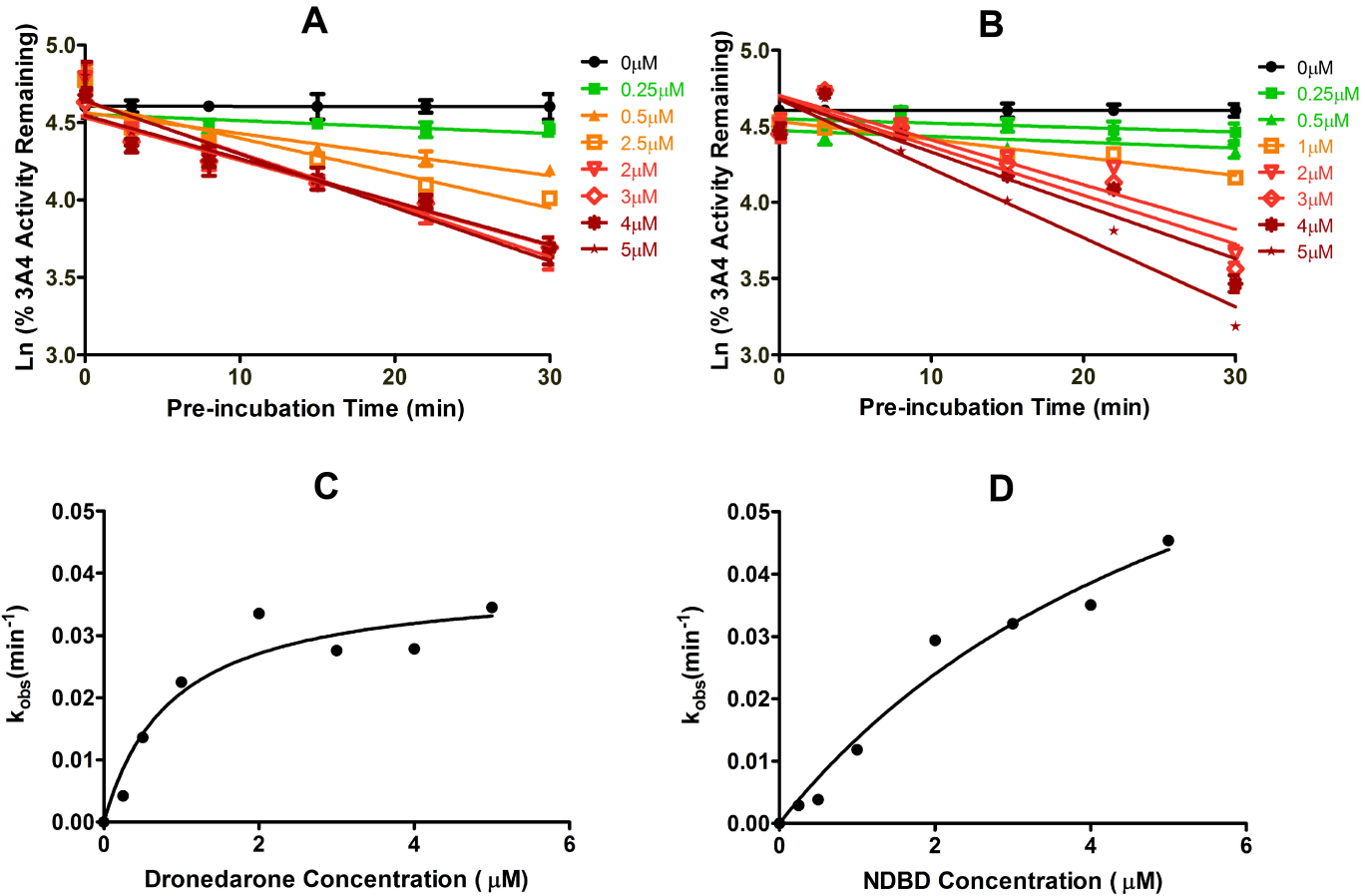
A
Ln (% 3A4 Activity Remaining)
5.0
4.5
4.0
3.5
3.0
0
10
20
30
Pre-incubation Time (min)
0μM
0.25μM
0.5μM
2.5μM
2μM
3μM
4μM
5μM
B
Ln (% 3A4 Activity Remaining)
5.0
4.5
4.0
3.5
3.0
0
10
20
30
Pre-incubation Time (min)
0μM
0.25μM
0.5μM
1μM
2μM
3μM
4μM
5μM
C
kobs(min-1)
0.05
0.04
0.03
0.02
0.01
0.00
0
2
4
6
Dronedarone Concentration (μM)
D
kobs(min-1)
0.05
0.04
0.03
0.02
0.01
0.00
0
2
4
6
NDBD Concentration (μM)

Figure 5

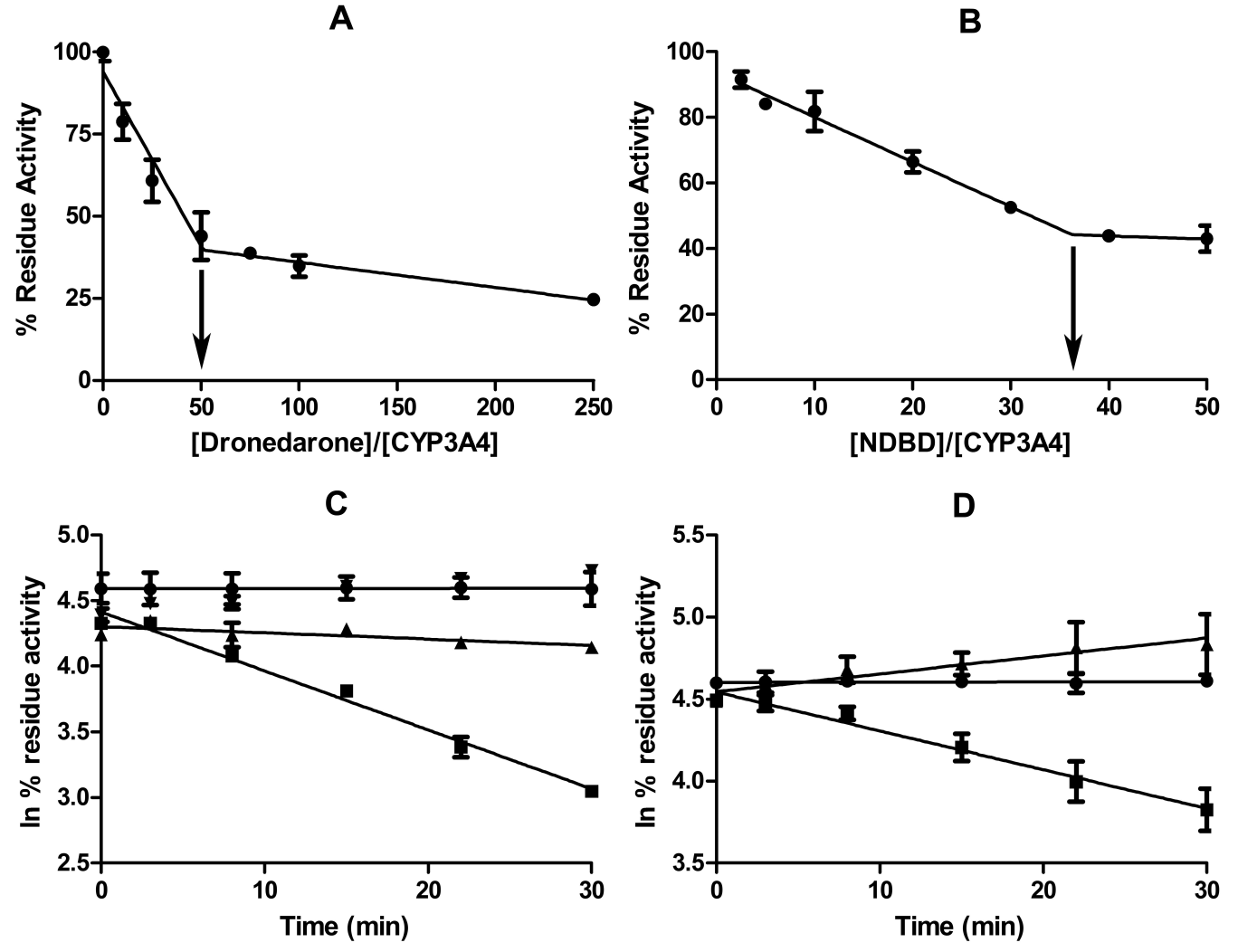
A
% Residue Activity
100
75
50
25
0
0
50
100
150
200
250
[Dronedarone]/[CYP3A4]
B
% Residue Activity
100
80
60
40
20
0
0
10
20
30
40
50
[NDBD]/[CYP3A4]
C
ln % residue activity
5.0
4.5
4.0
3.5
3.0
2.5
0
10
20
30
Time (min)
D
ln % residue activity
5.5
5.0
4.5
4.0
3.5
0
10
20
30
Time (min)

Figure 6

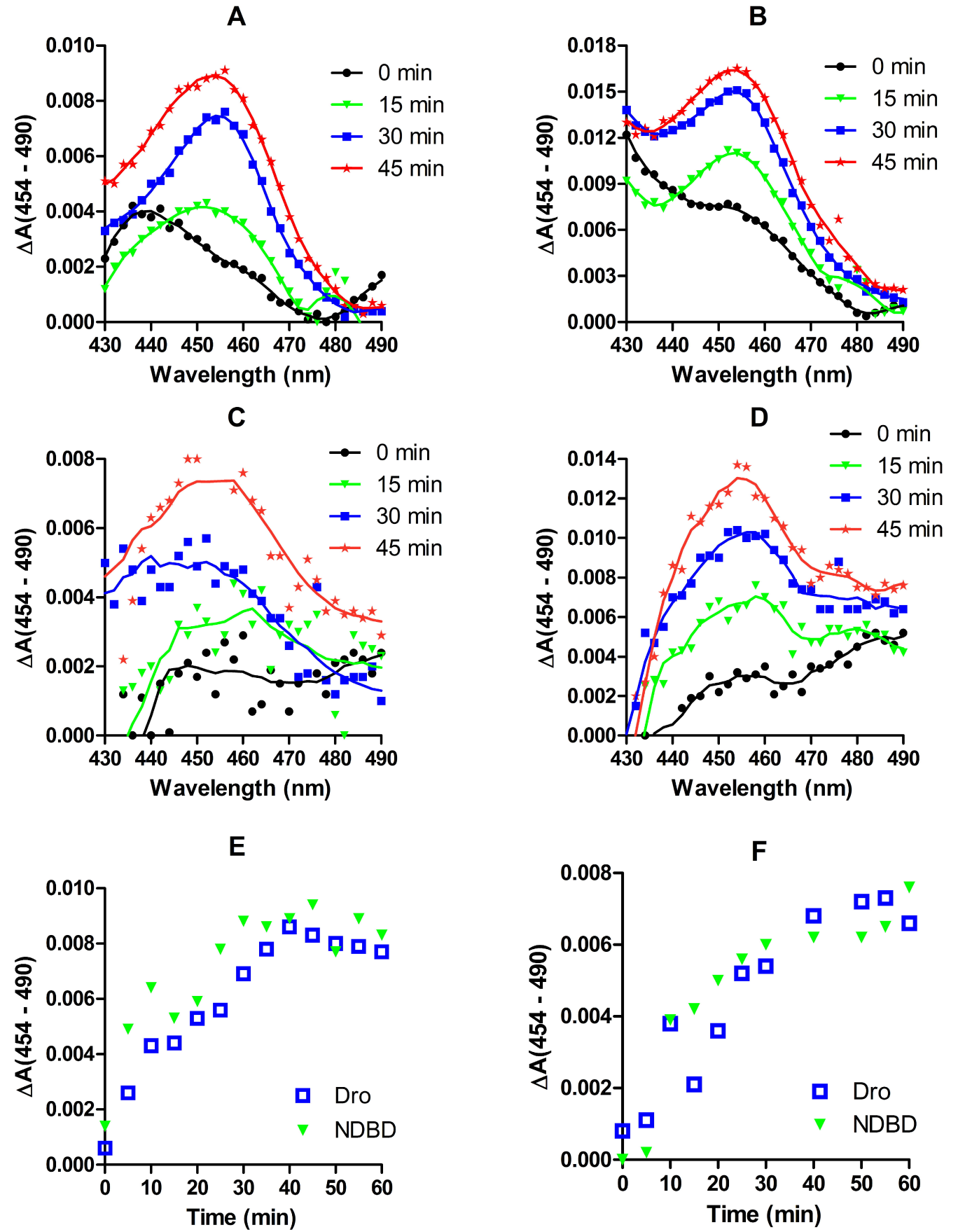
A
B
C
D
E
F
0 min
15 min
30 min
45 min
ΔA(454 - 490)
Wavelength (nm)
Time (min)
Dro
NDBD

Figure 7

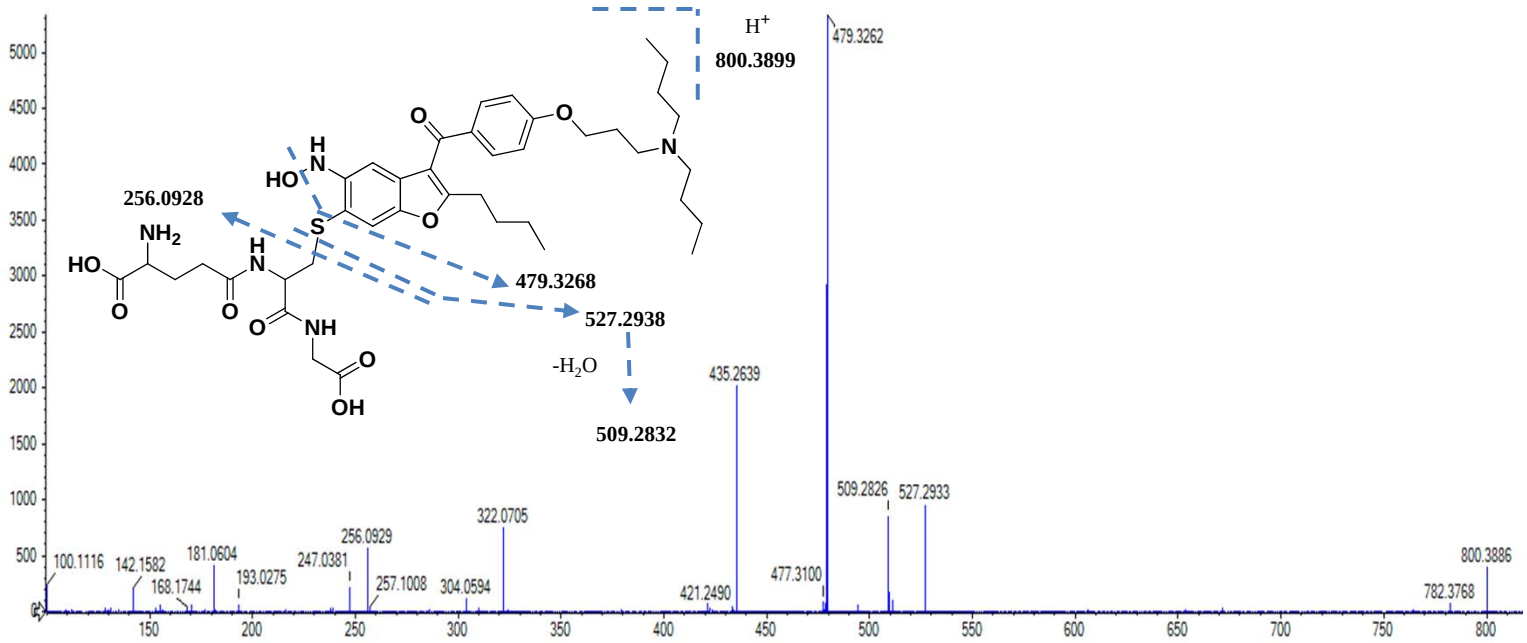

Molecular Pharmacology Fast Forward. Published on October 21, 2015 as DOI: 10.1124/mol.115.100891
This article has not been copyedited and formatted. The final version may differ from this version.

Figure 8